Assessing the performance of trajectory surface hopping methods: Ultrafast internal conversion in pyrazine

Weiwei Xie [iD], Marin Sapunar [iD], Nađa Došlić [iD], Matthieu Sala, and Wolfgang Domcke [iD]

View Online   **Export Citation**   **CrossMark**

ARTICLES YOU MAY BE INTERESTED IN

Direct quantum dynamics using variational Gaussian wavepackets and Gaussian process regression
The Journal of Chemical Physics **150**, 041101 (2019); https://doi.org/10.1063/1.5086358

Radical pair intersystem crossing: Quantum dynamics or incoherent kinetics?
The Journal of Chemical Physics **150**, 151102 (2019); https://doi.org/10.1063/1.5095204

Unsupervised machine learning in atomistic simulations, between predictions and understanding
The Journal of Chemical Physics **150**, 150901 (2019); https://doi.org/10.1063/1.5091842

Assessing the performance of trajectory surface hopping methods: Ultrafast internal conversion in pyrazine

View Online   Export Citation   CrossMark

Weiwei Xie,[1,2,3,a)] 🆔 Marin Sapunar,[4] 🆔 Nađa Došlić,[4,b)] 🆔 Matthieu Sala,[5] and Wolfgang Domcke[1,c)] 🆔

AFFILIATIONS

[1] Department of Chemistry, Technical University of Munich, Lichtenbergstr. 4, 85747 Garching, Germany
[2] Institute of Biological Interfaces (IBG-2), Karlsruhe Institute of Technology, 76131 Karlsruhe, Germany
[3] Institute of Physical Chemistry, Karlsruhe Institute of Technology, Kaiserstr. 12, 76131 Karlsruhe, Germany
[4] Department of Physical Chemistry, Ruđer Bošković Institute, HR-10000 Zagreb, Croatia
[5] Laboratoire Interdisciplinaire Carnot de Bourgogne UMR 6303 CNRS, Université de Bourgogne, BP 47870, F-21078 Dijon, France and Institut für Physikalische Chemie, Christian-Albrechts-Universität zu Kiel, Olshausenstr. 40, D-24098 Kiel, Germany

a) weiwei.xie@kit.edu
b) Nadja.Doslic@irb.hr
c) domcke@ch.tum.de

ABSTRACT

Trajectory surface hopping (TSH) methods have been widely used to study photoinduced nonadiabatic processes. In the present study, nonadiabatic dynamics simulations with the widely used Tully's fewest switches surface hopping (FSSH) algorithm and a Landau-Zener-type TSH (LZSH) algorithm have been performed for the internal conversion dynamics of pyrazine. The accuracy of the two TSH algorithms has been critically evaluated by a direct comparison with exact quantum dynamics calculations for a model of pyrazine. The model comprises the three lowest excited electronic states ($B_{3u}(n\pi^*)$, $A_{1u}(n\pi^*)$, and $B_{2u}(\pi\pi^*)$) and the nine most relevant vibrational degrees of freedom. Considering photoexcitation to the diabatic $B_{2u}(\pi\pi^*)$ state, we examined the time-dependent diabatic and adiabatic electronic population dynamics. It is found that the diabatic populations obtained with both TSH methods are in good agreement with the exact quantum results. Fast population oscillations between the $B_{3u}(n\pi^*)$ and $A_{1u}(n\pi^*)$ states, which reflect nonadiabatic electronic transitions driven by coherent dynamics in the normal mode Q_{8a}, are qualitatively reproduced by both TSH methods. In addition to the model study, the TSH methods have been interfaced with the second-order algebraic diagrammatic construction *ab initio* electronic-structure method to perform full-dimensional on-the-fly nonadiabatic dynamics simulations for pyrazine. It is found that the electronic population dynamics obtained with the LZSH method is in excellent agreement with that obtained by the FSSH method using a local diabatization algorithm. Moreover, the electronic populations of the full-dimensional on-the-fly calculations are in excellent agreement with populations of the three-state nine-mode model, which confirms that the internal conversion dynamics of pyrazine is accurately represented by this reduced-dimensional model on the time scale under consideration (200 fs). The original FSSH method, in which the electronic wave function is propagated in the adiabatic representation, yields less accurate results. The oscillations in the populations of the diabatic $B_{3u}(n\pi^*)$ and $A_{1u}(n\pi^*)$ states driven by the mode Q_{8a} are also observed in the full-dimensional dynamics simulations.

I. INTRODUCTION

The vast majority of chemistry relies on the Born-Oppenheimer (BO) approximation, that is, on the assumption that the electronic and nuclear motions can be separated. Within the BO approximation, the nuclei move on a single adiabatic potential energy surface (PES) provided by the electrons. In photoinduced processes, the BO approximation often breaks down and the nuclear motion

takes place on several coupled PESs. An important reason for the breakdown of the BO approximation is the existence of conical intersections (CI).[1–4] These are subspaces of the nuclear configuration space in which two or more electronic states become degenerate and which allow efficient population transfer between different electronic PESs.[5]

The theoretical study of photoinduced processes requires having at hand accurate and efficient methods for the description of nuclear motion on coupled multidimensional PESs. In the past few decades, a number of nonadiabatic dynamics methods have been developed which differ in the accuracy with which nuclear motion is treated.[6–9] The multi-configuration time-dependent Hartree (MCTDH) method is a well-established approach for the numerical solution of the time-dependent Schrödinger equation (TDSE) for nuclear motion.[6,10] In MCTDH, the multidimensional wave function is expanded in a time-dependent basis of so-called single-particle functions (SPF). This time-dependent basis yields a compact representation of the evolving wave packet which can result in substantial computational savings. This renders MCTDH the method of choice for treating the dynamics of multidimensional systems in which nuclear quantum effects cannot be neglected.[11–16] Importantly, the MCTDH method can provide benchmark results for assessing the accuracy of approximate methods.[17–19] The major drawback of the grid-based MCTDH approach is the necessity of precalculating and interpolating multidimensional PESs which cover the chemically relevant portion of the full-dimensional nuclear configuration space. Very recently, it has been shown that the MCTDH method can be implemented without the prior computation of global electronic PESs using machine learning techniques.[20,21]

There exist nonadiabatic quantum molecular dynamics methods which bypass the computation of PESs,[9] such as the *ab initio* multiple spawning (AIMS) method[2,22–24] and direct-dynamics versions of the variational multi-configurational Gaussian (vMCG) method.[25,26] These methods are gaining increasing popularity.[27–31] In the AIMS method, the nuclear wave function is expanded in a linear combination of time-dependent Gaussian basis functions which follow classical trajectories. The expansion coefficients are determined from the time-dependent Schrödinger equation and the spawning algorithm ensures that the nonadiabatic process is adequately described by introducing new basis functions, i.e., by spawning new ones. In the vMCG method, the TDSE for the expansion coefficients is solved variationally in a basis of time-dependent Gaussian basis functions. These methods are suitable to describe nuclear tunneling effects.[26] It goes without saying that the cost of performing these quantum molecular dynamics calculations is high.

In photochemical reactions, the time-dependent population probabilities of electronic states are usually the observables of interest and major quantum effects arise from the nondiabatic population transfer between electronic states. Trajectory-based mixed quantum-classical methods which account for switching between electronic states, but otherwise neglect nuclear quantum effects, are well suited to deliver this information. In trajectory surface hopping (TSH) methods,[8,32] trajectories evolve independently of each other, each of them in a given electronic state. Energies and forces are computed on the fly.[2,7,33,34] At given time steps, the surface

hopping (SH) algorithm determines whether the active state is changed or not. Tully's fewest switches (FS) algorithm relates the switching probability from the active electronic state i to another state j to the flux of population determined from the time-dependent electronic wave function.[35] Recently, practical solutions have been proposed to correct shortcomings of the original algorithm such as overcoherence[36–41] or numerical problems such as the identification of trivial crossings where the trajectory should follow the diabatic state.[42–44] These improvements as well as the inherent versatility and applicability to a wide range of different chemical problems render the fewest switches surface hopping (FSSH) method the most widely used SH algorithm.

Within the framework of independent trajectory calculations for several electronic states, one also can apply the time-honored Landau-Zener (LZ) formula[45–47] for the estimation of the SH probability. Although less popular than the FS algorithm, the LZ model has been widely employed in the seventies and eighties in atomic and molecular collision dynamics.[3,48,49] Among other applications, it was used by Tully and Preston in the first TSH calculation for the H + D$_2$ reaction.[32] The semiclassical LZ formula relates the transition probability between electronic states to the shape of the diabatic PESs in the vicinity of energy crossings rather than to the time-dependent electronic wave function. Therefore, (i) the so-called "lack of decoherence" problem of the FSSH method does not arise in this approach, (ii) it may be computationally more efficient, since the propagation of the TDSE is not required, and (iii) electronic-structure methods can be employed which provide only energies, but not wave functions, such as propagator methods or density functional theory. The diabatic formulation of the LZ formula does not lend itself readily to be implemented in on-the-fly TSH computations. However, a recent reformulation of the LZ hopping probability in terms of adiabatic potentials opened the door to straightforward on-the-fly Landau-Zener-type TSH (LZSH) computations.[50]

Recently, Xie and Domcke evaluated the performance of the FSSH and LZSH algorithms in comparison with exact nonadiabatic quantum dynamics calculations for a three-state two-mode model of the photoinduced hydrogen-atom detachment reaction in phenol.[51] They found that both algorithms give similar results, but failed to reproduce the time-dependent populations of the $^1\pi\pi^*$ and $^1\pi\sigma^*$ states or the branching ratio of the two electronic dissociation channels. Because the photodissociation of phenol involves nonadiabatic H-atom tunneling, it was difficult to judge the performance of the two algorithms due to the inherent inability of TSH to describe nonadiabatic tunneling effects.[52,53] Several other studies performed on low-dimensional model Hamiltonians also found that the neglect of nuclear quantum effects, such as the quantization of energy levels, which is directly related to problem of defining accurate initial conditions, quantum interference, or tunneling significantly affect the quality of trajectory-based simulations.[35,50,51,54–56]

Low-dimensional models, however, may not be representative for complex polyatomic systems. Therefore, the goal of this work is to assess the accuracy of the FSSH and LZSH algorithms beyond low-dimensional models. The performance of the two algorithms will be evaluated for one of the theoretically most extensively studied photophysical processes—the internal conversion in pyrazine after the excitation to the $B_{2u}(\pi\pi^*)$ state. The absorption

spectrum of pyrazine is characterized by a broad band in the region between 230 and 280 nm assigned to the $B_{2u}(\pi\pi^*)$ state.[57–59] Early theoretical studies predicted that an easily accessible CI between the $B_{2u}(\pi\pi^*)$ and $B_{3u}(n\pi^*)$ states leads the ultrafast decay of the former.[60–64] Time-resolved photoelectron spectroscopy experiments confirmed the theoretical predictions revealing a very short lifetime of the $B_{2u}(\pi\pi^*)$ state of about 20 fs.[65,66] Low-dimensional model Hamiltonians captured the essence of the $B_{2u}(\pi\pi^*)$ decay, but several aspects of the dynamics remained unclear. Recently, new insight into the excited-state dynamics of pyrazine was obtained from TDDFT-based FSSH studies which predicted the transient population of the dark $A_{1u}(n\pi^*)$ and $B_{2g}(n\pi^*)$ states.[67,68] To investigate the role of these excited states in the photodynamics of pyrazine, Sala *et al.* using multi-configuration multi-reference electronic-structure methods, constructed vibronic coupling model Hamiltonians encompassing two, three, and four excited electronic states and up to sixteen vibrational modes.[69] They performed nonadiabatic nuclear dynamics simulations with the MCTDH method and found that the nonadiabatic decay of the $B_{2u}(\pi\pi^*)$ state is governed by the competition of two decay pathways, one proceeding through the $B_{2u}(\pi\pi^*)/A_{1u}(n\pi^*)$ CI and the other through the well-established $B_{2u}(\pi\pi^*)/B_{3u}(n\pi^*)$ CI. It was found that the $B_{2g}(n\pi^*)$ state plays a minor role in the dynamics. The two-state and three-state vibronic coupling model Hamiltonians and the benchmark MCTDH study of Sala *et al.*[69] are an ideal opportunity for comparing the performance of the LZSH and FSSH algorithms for nonadiabatic dynamics simulations at CIs. In addition, we performed full-dimensional *ab initio* on-the-fly TSH simulations using the computationally efficient second-order algebraic diagrammatic construction (ADC(2)) method, in which we explored to what extent TSH methods are capable of capturing the intricate features of the nonadiabatic dynamics associated with multiple CIs in pyrazine. On the basis of these calculations we are not only able to compare the two algorithms but also to critically evaluate the accuracy of the three-state nine-mode vibronic coupling model which is an interesting research topic *per se*.

II. THE MODEL

The three-state model developed by Sala *et al.*[69] includes the three lowest excited states of pyrazine, the $B_{3u}(n\pi^*)$ state, the dark $A_{1u}(n\pi^*)$ state, and the bright $B_{2u}(\pi\pi^*)$ state. The nine vibrational normal modes included in the model are the four most important totally symmetric tuning modes (Q_{6a}, Q_1, Q_{9a}, Q_{8a}), which modulate the interstate energy gaps, and five non-totally symmetric coupling modes (Q_{10a}, Q_4, Q_5, Q_3, Q_{8b}). The couplings of the $B_{2u}(\pi\pi^*)$ state with the $B_{3u}(n\pi^*)$ and $A_{1u}(n\pi^*)$ states are mediated by the Q_{10a} and Q_4, Q_5 modes, respectively. The $B_{3u}(n\pi^*)$ and $A_{1u}(n\pi^*)$ states are coupled through the Q_3, Q_{8b} modes. The vibronic Hamiltonian is given in the diabatic representation as the sum of a reference Hamiltonian and a potential energy (PE) matrix

$$H(\boldsymbol{Q}) = H_0(\boldsymbol{Q}) + V^d(\boldsymbol{Q}), \tag{1}$$

where $\boldsymbol{Q}$ is the vector of dimensionless normal coordinates. The reference Hamiltonian is the ground-state Hamiltonian in the harmonic approximation

$$H_0 = \sum_i \frac{\omega_i}{2}\left(P_i^2 + Q_i^2\right)\boldsymbol{I}, \tag{2}$$

where P_i is the momentum operator of the ith normal coordinate and ω_i is the corresponding harmonic vibrational frequency. The diagonal and off-diagonal terms of the diabatic PE matrix $V^d(\boldsymbol{Q})$ are

$$V_{nn}^d(\boldsymbol{Q}) = E_n + \sum_i \kappa_i^n Q_i + \sum_j \gamma_j^n Q_j^2 \tag{3}$$

and

$$V_{nn'}^d(\boldsymbol{Q}) = \sum_k \lambda_k^{nn'} Q_k, \tag{4}$$

where n and n' denote electronic states, κ_i^n is the linear intrastate coupling constant of the ith totally symmetry mode in the nth electronic state, γ_j^n is the quadratic intrastate coupling constant of the jth non-totally symmetry mode in the nth electronic state and $\lambda_k^{nn'}$ is the linear interstate coupling constant between the nth and n'th electronic state. The features of the diabatic PE surfaces are discussed in Sec. IV.

The diagonalization of the matrix $V^d(\boldsymbol{Q})$

$$V^a(\boldsymbol{Q}) = U^\dagger(\boldsymbol{Q})V^d(\boldsymbol{Q})U(\boldsymbol{Q}) \tag{5}$$

yields the diagonal matrix with the adiabatic energies, $V^a(\boldsymbol{Q})$, and the transformation matrix $U(\boldsymbol{Q})$ which relates the adiabatic and diabatic wavefunction as

$$\psi^a(\boldsymbol{Q}) = U(\boldsymbol{Q})\psi^d(\boldsymbol{Q}). \tag{6}$$

In addition to the three-state model, we also consider the dynamics of a further simplified model (henceforth referred to as two-state model) including the $B_{3u}(n\pi^*)$ and $B_{2u}(\pi\pi^*)$ electronic states, four totally symmetric modes, and the single coupling mode Q_{10a}. We note that similar two-state three-mode models of pyrazine have extensively been used as benchmark models to test the accuracy of various trajectory-based methods.[70–73]

III. THEORETICAL AND COMPUTATIONAL METHODS

A. Landau-Zener surface hopping

In the framework of the LZSH method, introduced by Tully and Preston,[32] the nonadiabatic transition probability between two adiabatic electronic states j and k is given by the LZ formula[45–47]

$$P_{LZSH}^{j \to k} = \exp\left(-\frac{2\pi H_{jk}^2}{\hbar\dot{\boldsymbol{R}}|\boldsymbol{H}'_{jj} - \boldsymbol{H}'_{kk}|}\right), \tag{7}$$

where H_{jj} and H_{kk} are diagonal matrix elements of the electronic Hamiltonian which depend linearly on the vector of nuclear coordinates, H_{jk} is a constant off-diagonal matrix element, $\boldsymbol{H}'_{jj}$ and $\boldsymbol{H}'_{kk}$ denote derivatives with respect to nuclear coordinate $\boldsymbol{R}$, and $\dot{\boldsymbol{R}}$ is the velocity vector.

Without any approximation, the diabatic LZ formula [Eq. (7)] can be expressed in terms of the adiabatic PEs as[50]

$$P_{LZSH}^{j \to k} = \exp\left(-\frac{\pi}{2\hbar}\sqrt{\frac{Z_{jk}^3}{\ddot{Z}_{jk}}}\right), \tag{8}$$

where $\ddot{Z}_{jk}$ is the second-order time derivative of the absolute adiabatic energy gap Z_{jk} between two electronic states. In the present implementation, $\ddot{Z}_{jk}$ is evaluated by the three-point finite difference formula. In its adiabatic form, the LZ formula becomes a practical tool for computing SH probabilities in on-the-fly TSH calculations.[55] During the dynamics simulations, the absolute adiabatic energy gap is monitored at each time step. If a local minimum of the energy gap is attained, the hopping probability from the current adiabatic state j to another adiabatic state k is evaluated according to Eq. (8). A pseudorandom number uniformly generated from (0, 1) is compared with $P_{LZSH}^{j \to k}$ to determine whether the trajectory hops to a different state or continues in the current state. When a hopping event occurs, the momenta are adjusted by a scaling factor α, $\boldsymbol{P'} = \alpha \boldsymbol{P}$, to ensure the conservation of total energy

$$\frac{1}{2} \boldsymbol{P}^2 + V_j^a = \frac{1}{2} \alpha^2 \boldsymbol{P}^2 + V_k^a. \tag{9}$$

The specification of initial conditions in the LZSH calculations encompasses the initial coordinates and momenta of each trajectory and the specification of a single adiabatic state in which the dynamics is initialized. In the Condon approximation, the molecular wave function at $t = 0$, $|\Psi\rangle = |\chi_0\rangle|\psi_f^d\rangle$, is given as the product of the lowest vibrational state of the electronic ground state $|\chi_0\rangle$ and the excited diabatic state $|\psi_f^d\rangle$ since the dipole transition operator acts on the diabatic electronic wave function. The initial normal mode coordinates $\boldsymbol{Q_0}$ and momenta $\boldsymbol{P_0}$ were obtained from the Wigner distribution function[74]

$$\hat{W} = \int e^{\frac{i}{\hbar} \boldsymbol{P_0 S}} \int \langle \boldsymbol{Q_0} - \frac{\boldsymbol{S}}{2}|\chi_0\rangle\langle\chi_0|\boldsymbol{Q_0} + \frac{\boldsymbol{S}}{2}\rangle|\psi_f^d\rangle\langle\psi_f^d|d\boldsymbol{S}$$
$$= W(\boldsymbol{Q_0}, \boldsymbol{P_0})|\psi_f^d\rangle\langle\psi_f^d| \tag{10}$$

and then transformed to their Cartesian counterparts. To specify the initially excited adiabatic state, we employed the unitary transformation $\boldsymbol{U}$ between the diabatic and adiabatic representations [Eq. (6)] to obtain the Wigner distribution in the adiabatic basis

$$\hat{W} = W(\boldsymbol{Q_0}, \boldsymbol{P_0}) \sum_i |U_{fi}|^2 |\psi_i^a\rangle\langle\psi_i^a|. \tag{11}$$

The initially active adiabatic state is chosen randomly from the manifold of the adiabatic states $|\psi_i^a\rangle$ with the probability $|U_{fi}|^2$.

In the LZSH simulations, the adiabatic population probability of the state i is defined as the percentage of the trajectories propagating in the adiabatic state i

$$P_i^a(t) = \frac{N_i(t)}{N_{traj}}, \tag{12}$$

where $N_i(t)$ is the number of trajectories evolving on the adiabatic PES i and N_{traj} is the total number of trajectories. The LZSH and MCTDH results are most conveniently compared in the diabatic representation. Therefore, we transform the time-dependent adiabatic population probabilities obtained by the LZSH simulations to the diabatic representation. The population probability of the diabatic state i is given by transformation of the adiabatic projector to the diabatic representation

$$P_i^d(t) = \left[\boldsymbol{U}^{\dagger} \boldsymbol{P}^a \boldsymbol{U} \right]_{ii}, \tag{13}$$

where $\boldsymbol{P}^a$ is the adiabatic projector, i.e., a diagonal $n \times n$ matrix with unity at the position of active adiabatic state and zeros otherwise. $\boldsymbol{U}$ is given by Eq. (6).

B. Fewest switches surface hopping

In the FSSH method,[35] the electronic wave function evolves along the nuclear trajectory l according to the time-dependent Schödinger equation

$$i\hbar \frac{dC_j(\boldsymbol{R}^{(l)}(t))}{dt} = C_j(\boldsymbol{R}^{(l)}(t))V_j^a(\boldsymbol{R}^{(l)}(t))$$
$$- i\hbar \sum_k C_k(\boldsymbol{R}^{(l)}(t))\mathcal{D}_{jk}(\boldsymbol{R}^{(l)}(t)), \tag{14}$$

where the $C_j(\boldsymbol{R}^{(l)}(t))$ are the expansion coefficients of the electronic wave function in the adiabatic representation, $V_j^a(\boldsymbol{R}^{(l)}(t))$ is the PE of the jth adiabatic state and $\mathcal{D}_{jk}(\boldsymbol{R}^{(l)}(t))$ is the time derivative coupling (TDC) between the adiabatic electronic states j and k, which also can be written as

$$\mathcal{D}_{jk}(\boldsymbol{R}^{(l)}(t)) = \langle\psi_j(\boldsymbol{R}^{(l)}(t))|\frac{d}{dt}|\psi_k(\boldsymbol{R}^{(l)}(t))\rangle$$
$$= \dot{\boldsymbol{R}}^{(l)}(t)d_{jk}(\boldsymbol{R}^{(l)}(t)), \tag{15}$$

where $d_{jk}(\boldsymbol{R}^{(l)}(t))$ denotes the nonadiabatic coupling vector.

The essential criterion of the FSSH algorithm is the consistency of the number of trajectories evolving in the electronic state j, denoted N_j, with the average population $|C_j(\boldsymbol{R}^{(l)}(t))|^2$ of this state at time t in the electronic wave function, such that

$$\frac{N_j(t)}{N_{\text{traj}}} \approx \frac{1}{N_{\text{traj}}} \sum_l^{N_{\text{traj}}} \left| C_j(\boldsymbol{R}^{(l)}(t)) \right|^2. \tag{16}$$

The FSSH algorithm is designed to minimize the number of state switches in order to satisfy the consistency relation in such a way that hops between PESs occur only when the currently occupied state exhibits a reduction of population. The hopping probability is defined as

$$P_{FSSH}^{j \to k} = \max\left\{ 0, -\frac{d|C_{j \to k}(\boldsymbol{R}^{(l)}(t))|^2}{dt} \right\}$$
$$= \max\left\{ 0, \frac{2\mathcal{D}_{jk}(\boldsymbol{R}^{(l)}(t))Re\left[C_k^*(\boldsymbol{R}^{(l)}(t))C_j(\boldsymbol{R}^{(l)}(t)) \right]dt}{|C_j(\boldsymbol{R}^{(l)}(t))|^2} \right\}. \tag{17}$$

The maximum value criterion assures that the probability is always positive and hops only take place from the state undergoing depopulation. A uniform random number ξ between 0 and 1 is generated and a switch from state j to state k takes place, if

$$\sum_{i=1}^{k-1} P_{FSSH}^{j \to i} < \xi \le \sum_{i=1}^{k} P_{FSSH}^{j \to i}. \tag{18}$$

To ensure the conservation of total energy for each trajectory, the mass-weighted momenta are adjusted along the nonadiabatic coupling vector. In the present implementation of the FSSH

method, the nonadiabatic coupling vector is not explicitly evaluated, and the momenta are adjusted by a scaling factor α calculated by Eq. (9).

The time-dependent adiabatic and diabatic population probabilities are calculated by Eqs. (12) and (13), respectively. In the FSSH method, the diabatic/adiabatic populations can also be calculated as averages of the squares of the coefficients of the diabatic/adiabatic electronic wave functions over all trajectories. However, these two recipes do not provide identical results due to the lack of electronic decoherence (see Sec. III C 1) in the FSSH method.

C. Computational implementation

1. Surface hopping methods

In the two-state and three-state vibronic models, the initial conditions were randomly sampled from the Wigner distribution function given in Eq. (10). The initially populated electronic state was the diabatic $B_{2u}(\pi\pi^*)$ state. We distributed the trajectories among the adiabatic states according to Eq. (11). The classical equations of motion were integrated by the fourth-order Runge-Kutta algorithm with an integration time step 0.5 fs. Since the electronic Hamiltonian in the model studies is given in the diabatic representation, U is straightforwardly obtained by the diagonalization of the electronic Hamiltonian and the diabatic populations can be computed according to Eq. (13). All trajectories were propagated for 200 fs. A swarm of 1000 trajectories was sufficient to obtain converged averages of the observables. To avoid numerical inaccuracies caused by peaked nonadiabatic couplings at conical intersections, the TDSE in the FSSH method was propagated in the diabatic representation.

To perform full-dimensional *ab initio* on-the-fly TSH calculations for pyrazine, we interfaced the code with the ADC(2) electronic-structure method[75–78] implemented in Turbomole.[79] Initial geometries and momenta were sampled from the Wigner distribution function in the electronic ground state obtained from the Hessian matrix computed at the MP2/aug-cc-pVDZ level. The initial population probability of the adiabatic S_1, S_2, and S_3 excited states was sampled stochastically from the oscillator strengths of the adiabatic states. Since the dipole transition moments of the two diabatic $n\pi^*$ states (A_{1u} and B_{3u}) from the electronic ground state are very small compared with the transition dipole moment of the bright diabatic $B_{2u}(\pi\pi^*)$ state, the former transition moments can be set to zero. The initial population of the adiabatic excited states according to their oscillator strengths is then equivalent to the initial population of the diabatic B_{2u} state with probability unity and zero initial population in the diabatic A_{1u} and B_{3u} states. The sampling of the initial electronic states in the *ab initio* on-the-fly simulations is therefore identical to the initial sampling employed in the simulations for the three-state model. Newton's equations were integrated with the velocity-Verlet algorithm using a time step of 0.5 fs. For each initial sample of adiabatic population probability, coordinates, and momenta, 500 trajectories were launched and propagated in the electronic subspace spanned by the electronic ground state and the four lowest excited electronic states for 200 fs. Taking account of the orthogonality of the diabatic-to-adiabatic transformation matrix U in Eq. (6) and the fact that the transition dipole moments of the diabatic A_{1u} and B_{3u} states are zero, the matrix U can be

reconstructed at each nuclear geometry from the oscillator strengths f_{01}, f_{02}, f_{03} of the adiabatic electronic states. With this local matrix U, the adiabatic population probabilities at time t, given by the fraction of trajectories in each adiabatic state, can be transformed to the diabatic electronic populations at time t. This back-transformation yields the time-dependent diabatic electronic population probabilities which can directly be compared with the diabatic electronic population probabilities obtained with quantum wave-packet calculations.

It is well known that the FSSH algorithm suffers from a number of shortcomings, including lack of decoherence and numerical inaccuracies that can arise in the propagation of the TDSE in the adiabatic representation due to strongly peaked nonadiabatic coupling elements at conical intersections. Because the TDSE for the electronic wave function is solved using a single trajectory, the FSSH method tends to overestimate electronic coherence. Several recipes have been proposed for reducing the electronic coherence.[36–41] Owing to its simplicity, we employed in the FSSH calculations the empirical correction of Granucci and Persico[40] with a correction parameter $\alpha = 0.1$ E_h. In general, the effect of the decoherence correction is minor on the time scales considered in the present work (200 fs). A comparison of electronic state populations calculated with the FSSH method with and without decoherence corrections is provided in Sec. II of the supplementary material.

In the FSSH method, the time derivative couplings (TDCs) are needed for the integration of the electronic TDSE in the adiabatic representation. The TDCs exhibit singularities at CIs which can cause numerical inaccuracies in the propagation of the electronic wave function. To identify possible numerical inaccuracies, we implemented two versions of *ab initio* on-the-fly FSSH simulations. In the first implementation (i), the electronic wave function was propagated in the adiabatic representation and the TDCs were determined from the overlap of electronic wave functions using the norm-preserving interpolation algorithm of Meek and Levine.[80] This implementation of the FSSH method is denoted as A-FSSH in the following. In the second implementation (ii) of the FSSH method in the *ab initio* on-the-fly simulations, the electronic wave function was propagated in a locally diabatic representation as proposed by Granucci *et al.*[81] This implementation is referred to as LD-FSSH in what follows. A more detailed description of these integration schemes is given in Sec. I of the supplementary material.

2. Quantum dynamics method

Benchmark quantum dynamics calculations were performed using the MCTDH method. The MCTDH method is an efficient grid-based method to solve the nuclear TDSE designed to study multi-dimensional problems. In MCTDH, the wavefunction is expanded in a contracted basis of time-dependent functions called single-particle functions (SPF), which is determined variationally from an underlying direct-product primitive basis. Detailed descriptions of the method have been published elsewhere, see Refs. 6 and 10. The calculations were performed in the so-called multi-set formalism, in which different sets of SPF basis functions are used to describe the nuclear wavepackets on different electronic states.[82] A Hermite polynomial discrete variable representation (DVR)[83] primitive basis was used for all nuclear degrees of freedom. The numbers

TABLE I. Number of SPF and primitive basis functions used in the MCTDH calculations.

Model	Combinations of modes	Numbers of SPFs	Numbers of grid points
Two-state	$(\nu_{6a}, \nu_{10a}), \nu_1$	[26,17], [8,6],	(36,40), 26
	ν_{9a}, ν_{8a}	[5,4], [5,4]	18, 24
Three-state	$(\nu_{6a}, \nu_{10a}), (\nu_1, \nu_4),$	[34,40,17], [15,18,10],	(42,48), (26,24),
	$(\nu_{9a}, \nu_3, \nu_{8b}), (\nu_{8a}, \nu_5)$	[20,22,11], [21,25,10]	(20,14,22), (30,14)

of primitive and SPF basis functions used in the calculations for the two-state and three-state models are given in Table I. In each calculation, the initial condition for the time propagation was constructed by vertical excitation, i.e., by the transfer of the vibrational ground state of the S_0 state to the diabatic $B_{2u}(\pi\pi^*)$ electronic state. The constant mean field integration scheme[84] with an initial step size of 0.01 fs and an error tolerance of 10^{-7} was used.

IV. RESULTS AND DISCUSSION

A. Electronic structure calculations

Figures 1(a)–1(d) display one-dimensional cuts of the diabatic PESs of the lowest three excited states of pyrazine along the four most relevant dimensionless tuning modes, calculated with the XMCQDPT2/aug-cc-pVDZ method.[85] The results of the accurate but computationally expensive multi-reference XMCQDPT2 method serve as benchmarks for the estimation of the accuracy of the computationally less expensive single-reference ADC(2) method. In the energy scan along the Q_{6a} mode [Fig. 1(a)], the position of the CI between the $B_{2u}(\pi\pi^*)$ and $B_{3u}(n\pi^*)$ states ($Q_{6a} = -1.0$) is

more than three times further from the ground-state equilibrium geometry than the position of the $B_{2u}(\pi\pi^*)/A_{1u}(n\pi^*)$ CI. On the other hand, the coupling of the $B_{2u}(\pi\pi^*)$ state with the $B_{3u}(n\pi^*)$ state is stronger than the coupling with the $A_{1u}(n\pi^*)$ state.[69] This implies that after excitation to the $B_{2u}(\pi\pi^*)$ state, internal conversion to the $B_{3u}(n\pi^*)$ state is in competition with internal conversion to the $A_{1u}(n\pi^*)$ state. Figure 1(d) presents the energy scan along the Q_{8a} mode and shows the existence of a $A_{1u}(n\pi^*)/B_{3u}(n\pi^*)$ CI. It has been found in recent quantum dynamics calculations[69] that this CI is responsible for population oscillations between the $A_{1u}(n\pi^*)$ and $B_{3u}(n\pi^*)$ states after the decay from the $B_{2u}(\pi\pi^*)$ state.

A comparison of the ADC(2) vertical excitation energies of the four lowest excited states with previous calculations as well as experimental data is shown in Table II. The 0-0 transition energy of the $B_{3u}(n\pi^*)$ state at the ADC(2)/aug-cc-pVDZ level is 4.05 eV, 0.22 eV higher than the experimental value of 3.83 eV.[86] The ADC(2) vertical excitation energy of the $B_{3u}(n\pi^*)$ state is 0.16 (0.25) eV higher than the vertical excitation energy of the $B_{3u}(n\pi^*)$ state at the CASPT2[87] (XMCQDPT2[69]) level. The 0-0 transition energy and the vertical excitation energy of the $B_{2u}(\pi\pi^*)$ state at the ADC(2)/aug-cc-pVDZ
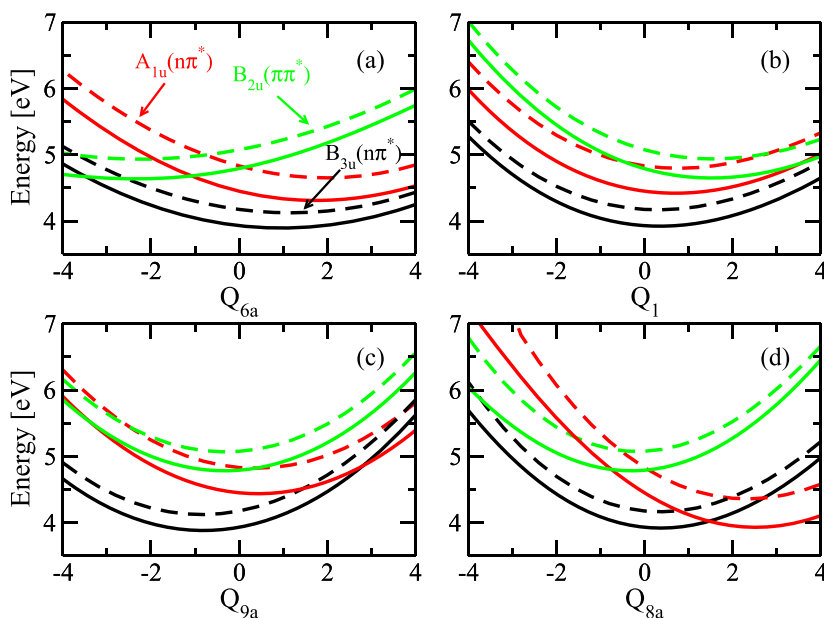

FIG. 1. One-dimensional cuts of the potential energy surfaces of the $B_{3u}(n\pi^*)$ (black), $A_{1u}(n\pi^*)$ (red), and $B_{2u}(\pi\pi^*)$ (green) states along the four most important totally symmetric dimensionless normal modes, Q_{6a} (a), Q_1 (b), Q_{9a} (c), Q_{8a} (d). The full and dashed lines represent the XMCQDPT2/aug-cc-pVDZ and ADC(2)/aug-cc-pVDZ results, respectively.

TABLE II. Vertical excitation energies (in eV) computed with the ADC(2)/aug-cc-pVDZ(AVDZ) method compared with previous theoretical results and experimental data. The 0-0 transition energies are given in parentheses.

	$B_{3u}(n\pi^*)$	$A_{1u}(n\pi^*)$	$B_{2u}(\pi\pi^*)$	$B_{2g}(n\pi^*)$
Expt.[86]	$-(3.83)$	...	$4.81^a(4.69^b)$	...
ADC(2)/AVDZ	4.18(4.05)	4.83	5.08(4.81)	5.85
CASPT2/AVTZ[87]	4.02	4.75	4.80	5.56
XMCQDPT2/AVDZ[69]	3.93	4.45	4.79	5.38
CC2/TZVP[88]	4.26	4.95	5.13	5.92
CC3/TZVP[88]	4.24	5.05	5.02	5.74
TDDFT/B3LYP/TZVP[67]	3.96	4.6	5.46	6.3

[a]Band maximum.
[b]0-0 transition.

level are found to be 0.12 eV and 0.27 eV, respectively, higher than the experimental values.[86] The ADC(2) $B_{2u}(\pi\pi^*)$ vertical excitation value of 5.08 eV is also in good agreement with the benchmark values of 4.80 eV and 4.79 eV obtained with the CASPT2 and XMC-QDPT2 methods. The CC2[88] and CC3[88] methods yield similar vertical excitation energies as the ADC(2) method, while the TDDFT method significantly overestimates the vertical excitation energy of the $B_{2u}(\pi\pi^*)$ state.[67]

In contrast to the consistent experimental data for the vertical excitation energy of the bright $B_{2u}(\pi\pi^*)$ bright state,[57,86,89] the vertical energy of the dark $A_{1u}(n\pi^*)$ state is controversial. Walker and Palmer reported an experimental value of 5.0 eV based on near-threshold electron-energy loss spectra.[90] On the other hand, the $A_{1u}(n\pi^*)$ state was not detected in a recent photoelectron imaging experiment by Suzuki and co-workers.[66] On the theoretical side, the location of the $A_{1u}(n\pi^*)$ state is sensitive to the electronic-structure method used for the calculation. The XMC-QDPT2, CC2, ADC(2) and TDDFT methods predict the $A_{1u}(n\pi^*)$ state below the $B_{2u}(\pi\pi^*)$ state, while the CASPT2 and CC3 calculations predict the $A_{1u}(n\pi^*)$ and $B_{2u}(\pi\pi^*)$ states to be essentially degenerate.
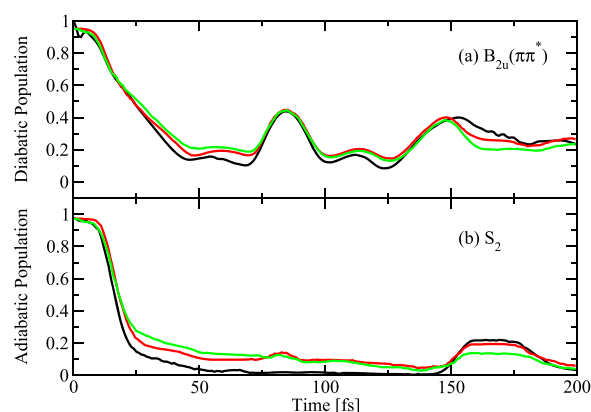
Similarly, the position of the dark $B_{2g}(n\pi^*)$ state is uncertain. Walker and Palmer[90] proposed an experimental value of 6.0 eV, while a UV-IR double resonance dip measurement by Okuzawa et al.[59] reported a much lower value of 5.19 eV. As seen in Table II, all computational results included in the table predict the energy of the $B_{2g}(n\pi^*)$ state to be significantly higher than the energy of the $B_{2u}(\pi\pi^*)$ state. This implies the $B_{2g}(n\pi^*)$ state should have a negligible influence on the nonadiabatic dynamics of pyrazine after photoexcitation to the $B_{2u}(\pi\pi^*)$ state.

The dashed lines in Figs. 1(a)–1(d) show one-dimensional PE cuts along four totally symmetric normal coordinates calculated at ADC(2)/aug-cc-pVDZ level. Overall, the PE functions calculated with the XMCQDPT2 and ADC(2) methods are nearly parallel along these normal coordinates. The crossings between the ADC(2) PE curves are located virtually at the same positions as those of the XMCQDPT2 calculations, which indicates that the ADC(2) method is a reliable and computationally efficient alternative to the XMC-QDPT2 method for on-the-fly dynamics calculations for the excited states of pyrazine.

B. Two-state model

We first consider the two-state model in which the couplings of the $A_{1u}(n\pi^*)$ state with the $B_{2u}(\pi\pi^*)$ and $B_{3u}(n\pi^*)$ states are switched off. Figure 2(a) shows the time-dependent population probability of the diabatic $B_{2u}(\pi\pi^*)$ state. The exact quantum mechanical result obtained with the MCTDH method is shown by the black curve. The population of the $B_{2u}(\pi\pi^*)$ state decays to a value of 0.15 within 45 fs and then exhibits recurrences with a period of about 60 fs. The recurrences reflect the coherent driving of the populations of the diabatic $B_{2u}(\pi\pi^*)$ and $B_{3u}(n\pi^*)$ states by wave-packet dynamics in the mode Q_{6a} [see Fig. 1(a)]. The population of the adiabatic S_2 state is displayed in Fig. 2(b). Compared to the diabatic population, the adiabatic population exhibits a faster decay on a time scale of about 30 fs and exhibits a single recurrence at 170 fs.

The population dynamics obtained with the LZSH and FSSH methods is shown by the red and green curves, respectively, in

FIG. 2. Populations of the diabatic $B_{2u}(\pi\pi^*)$ state (a) and the adiabatic S_2 state (b) for the two-state model. The black, red, and green lines are calculated with the multi-configuration time-dependent Hartree (MCTDH), Landau-Zener surface hopping (LZSH) and Tully's fewest switches surface hopping (FSSH) methods, respectively.

Figs. 2(a) and 2(b). Overall, the exact electronic population dynamics (black curve) is accurately reproduced by both TSH methods. The deviations between the FSSH and LZSH results are smaller than their deviations from the exact quantum results. The population recurrences in the diabatic $B_{2u}(\pi\pi^*)$ state and in the adiabatic S_2 state are qualitatively reproduced by both TSH methods. These findings demonstrate that the electronic population oscillations are the consequence of vibrational rather than electronic coherence. The latter cannot be reproduced by surface-hopping simulations.[91]

C. Three-state model

The diabatic electronic populations for the three-state model obtained with the numerically exact MCTDH method are shown as black lines in Figs. 3(a)–3(c). The population of the diabatic $B_{2u}(\pi\pi^*)$ state decays to almost zero on a time scale of 45 fs, in contrast to the relatively high value of 0.18 in the simulation for the two-state model. The population oscillations between the $B_{2u}(\pi\pi^*)$ and $B_{3u}(n\pi^*)$ states are suppressed by the coupling between the $B_{3u}(n\pi^*)$ and $A_{1u}(n\pi^*)$ states in the three-state model for two reasons. First, internal conversion from the $B_{2u}(\pi\pi^*)$ state to the $A_{1u}(n\pi^*)$ state reduces population transfer to the $B_{3u}(n\pi^*)$ state. Second, the wave packet in the $B_{3u}(n\pi^*)$ state passes through the $B_{3u}(n\pi^*)/A_{1u}(n\pi^*)$ CI and partly relaxes to the $A_{1u}(n\pi^*)$ state, reducing the components of wave packet in the $B_{2u}(\pi\pi^*)$ state. The populations of the diabatic $A_{1u}(n\pi^*)$ and $B_{3u}(n\pi^*)$ states, shown in Figs. 3(b) and 3(c), rise quickly during the first 30 fs, revealing the competition between the population transfers to the $A_{1u}(n\pi^*)$ and $B_{3u}(n\pi^*)$ states. After 40 fs, the diabatic population starts to oscillate between the $A_{1u}(n\pi^*)$ and $B_{3u}(n\pi^*)$ states. As discussed, the oscillations reflect nonadiabatic electronic transitions driven by coherent dynamics in the Q_{8a} mode.

The diabatic populations calculated with the LZSH method and FSSH methods are shown by red and green lines, respectively. Overall, both TSH results are in very good agreement with the exact results. The weak recurrences in the $B_{2u}(\pi\pi^*)$ population

and the quasi-periodic feature in the populations of the $B_{3u}(n\pi^*)$ and $A_{1u}(n\pi^*)$ states are qualitatively reproduced by both TSH methods.

Figures 4(a)–4(c) presents the adiabatic populations obtained with two TSH methods. In the MCTDH method, the time-dependent wave function is computed in the diabatic representation. Adiabatic electronic populations can be obtained by evaluating expectation values of projection operators on adiabatic states with the diabatic wave function, which is equivalent to a transformation from the diabatic to the adiabatic electronic basis.[6,10] It was not possible to obtain fully converged adiabatic electronic population probabilities with the MCTDH method for the model including three electronic states and nine nuclear degrees of freedom. Therefore, numerically exact reference adiabatic populations are not available for comparison in Fig. 4. The populations of the S_1, S_2 and S_3 states calculated with the LZSH and FSSH methods are in excellent agreement. At $t = 0$, the diabatic $B_{2u}(\pi\pi^*)$ state is populated, which corresponds to a 77%/21% population ratio of the adiabatic S_3 and S_2 states. The S_3 state population decays on a time scale of about 20 fs. The S_2 population calculated by the LZSH (FSSH) method rises to a maximum of 0.5 (0.4) within the first 15 fs, and then slowly transfers to the S_1 state. The increase of the S_1 population, on the other hand, is monotonous. After 60 fs, the population dynamics is essentially finished and about 20% and 80% of populations remain on the S_1 and S_2 states, respectively.

D. *Ab initio* on-the-fly simulations

Nonadiabatic on-the-fly dynamics simulations were performed with the ADC(2) method assuming instantaneous excitation of the optically bright diabatic $B_{2u}(\pi\pi^*)$ state. Since internal conversion to the ground state takes place on picosecond time scales,[92] this process is not considered in the present simulations covering 200 fs. The performance of the LZSH method has been compared with the A-FSSH and LD-FSSH methods.

Figures 5(a)–5(c) show the time-dependent populations of the three lowest adiabatic excited states, S_1, S_2, and S_3. At $t = 0$,
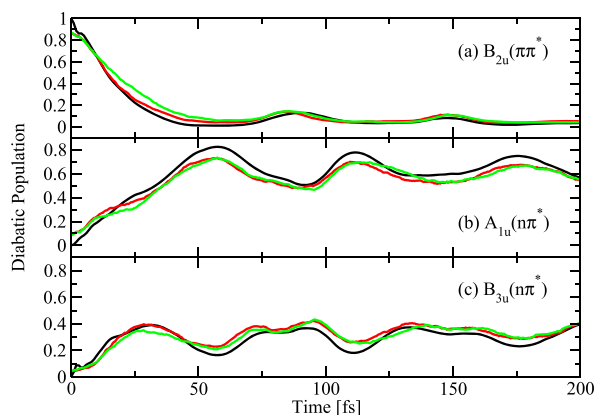
FIG. 3. Populations of the diabatic $B_{2u}(\pi\pi^*)$ (a), $A_{1u}(n\pi^*)$ (b) and $B_{3u}(n\pi^*)$ (c) states for the three-state model. The black, red, and green lines are calculated with the MCTDH, LZSH and FSSH methods, respectively.
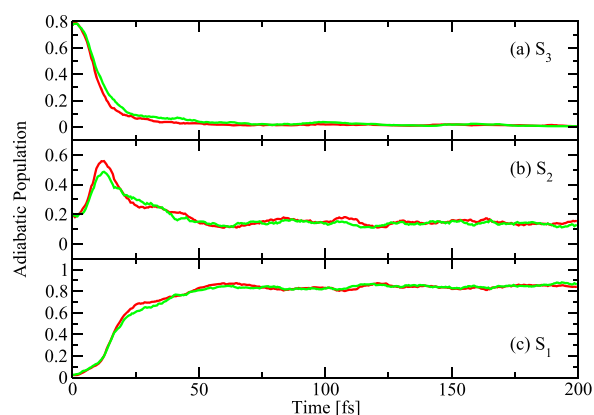
FIG. 4. Populations of the adiabatic S_3 (a), S_2 (b), and S_1 (c) states for the three-state model. The red and green lines are calculated with the LZSH and FSSH methods, respectively.
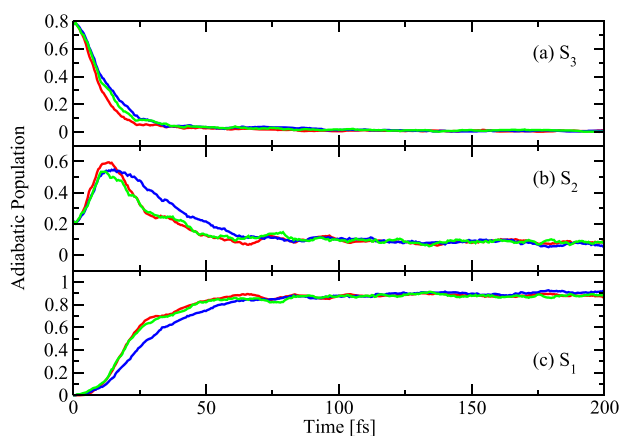
FIG. 5. Populations of the adiabatic S_3 (a), S_2 (b), and S_1 (c) states calculated with full-dimensional *ab initio* ADC(2) simulations. The red line shows the populations calculated with the LZSH method. The green and blue lines give the populations calculated with two versions of the FSSH method. In the LD-FSSH method (green), the electronic wave function is propagated in a locally diabatic basis. In the A-FSSH method (blue), the electronic wave function is propagated in the adiabatic representation using the norm-preserving scheme.

the diabatic $B_{2u}(\pi\pi^*)$ state is populated, which corresponds to a 78.5%/20.5% population ratio of the adiabatic S_2 and S_3 states. The initial population of the S_4 state is only 1.0%. In addition, the population of the S_4 state (not shown) attains a maximum of less than 0.03 during the course of the simulation, which further confirms that the $B_{2g}(n\pi^*)$ state plays a negligible role in the internal conversion dynamics of pyrazine. The S_3 state population decays to zero within a time scale of 25 fs. The population of the S_2 state calculated with the LZSH (LD-FSSH) method reaches a maximum value of 0.60 (0.55) at 14 (12) fs. The population of the S_1 state increases in the first 50 fs and then basically become constant. The overall population dynamics of full-dimensional pyrazine is similar to that obtained for the three-state nine-mode model (Fig. 4), indicating that this model comprises the relevant electronic states and vibrational modes governing the the internal conversion process of pyrazine.

Comparing the LZSH, A-FSSH, and LD-FSSH results, the LD-FSSH populations are in significantly better agreement with the LZSH results than the A-FSSH results. Apart from a slightly slower initial decay of the S_3 population and a somewhat lower maximum value of the S_2 population in the LD-FSSH result, the LZSH and LD-FSSH results are essentially identical (Fig. 5). The A-FSSH method underestimates the decay rate of the intermediate S_2 population and, correspondingly, the increase of the S_1 population. The sharply peaked nonadiabatic coupling at the S_2/S_1 CI is possibly not fully captured by the propagation of the electronic TDSE in this implementation of FSSH. In the long-time limit (200 fs), all three methods give the same electronic populations. We mention that the LD-FSSH method without decoherence corrections underestimates the asymptotic limit of the S_1 population (see Sec. II of the supplementary material).

To gain further insight into the performance of the TSH methods and differences between the LZSH, LD-FSSH, and A-FSSH

algorithms, we evaluated the dependence of the number of successful hops between the S_3 and S_2 states and S_2 and S_1 states on the instantaneous adiabatic energy gaps. As shown in Figs. 6(a) and 6(b), the distribution of the number of S_3–S_2 and S_2–S_1 hops is peaked at small energy gaps (~0.1 eV), which shows that most hopping events occur in the vicinity of CIs for all three algorithms. The LZSH distribution is somewhat more localized than the two FSSH distributions. In the LZSH calculations, no hopping events take place for S_2–S_1 energy gaps larger than 0.5 eV, in contrast to a substantial number of hops occurring in both FSSH methods. In close proximity of the S_3/S_2 and S_2/S_1 CIs (energy gap < 0.05 eV), the hops of the LD-FSSH method exhibit almost identical probability as the hops of the A-FSSH method. When the S_2–S_1 or S_3–S_2 energy gap is larger than 0.05 eV, the hopping probability of the A-FSSH method is lower than the hopping probability of the LD-FSSH method. This leads to slower increase of the rate of the adiabatic population of the S_1 state calculated with the A-FSSH method compared to the LD-FSSH method [see Fig. 5(c)]. The FSSH method in principle is more general than the LZSH method and presumably preferable in cases where the nuclear dynamics is not dominated by conical intersections or weakly avoided crossings. The LZSH method is most suitable for the simulation of ultrafast nonadiabatic dynamics occurring at or near conical intersections. One can anticipate that larger differences between the LZSH and FSSH simulations may arise in systems in which the probability of nonadiabatic transitions is small and hops take place at geometries in which the energy gap between adiabatic PESs is relatively large.

The populations of the diabatic $B_{2u}(\pi\pi^*)$, $A_{1u}(n\pi^*)$, and $B_{3u}(n\pi^*)$ states obtained with the LZSH and LD-FSSH methods are presented in Figs. 7(a)–7(c). Excellent agreement between the results of the LZSH and LD-FSSH methods is observed for the diabatic populations. The population of the $B_{2u}(\pi\pi^*)$ state decays monotonously with a time constant of 23 fs, in excellent agreement with the experimental measurement of 23 ± 4 fs.[66] The populations of the $A_{1u}(n\pi^*)$
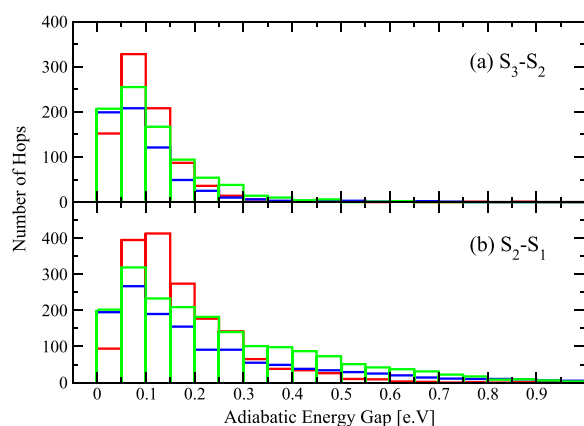

FIG. 6. Distribution of the number of successful hops between the S_3 and S_2 states (a) and the S_2 and S_1 states (b) vs the instantaneous energy gap in the full-dimensional ADC(2) simulations. The red, green, and blue lines were calculated with the LZSH, LD-FSSH and A-FSSH methods, respectively.
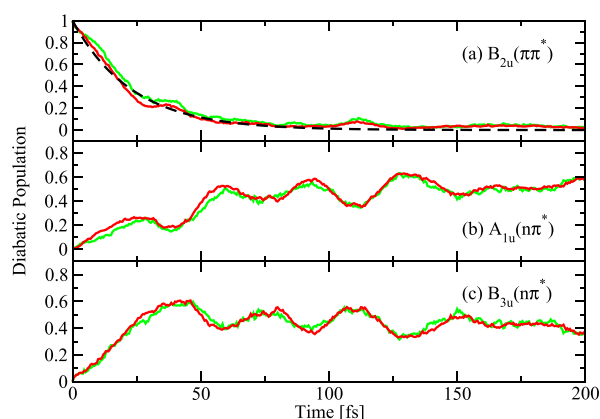
FIG. 7. Populations of the diabatic $B_{2u}(\pi\pi^*)$ (a), $A_{1u}(n\pi^*)$ (b), and $B_{3u}(n\pi^*)$ (c) states calculated with full-dimensional *ab initio* ADC(2) simulations. The red and green lines are calculated with the LZSH and LD-FSSH methods, respectively. The dashed line indicates the exponential fitting curve.
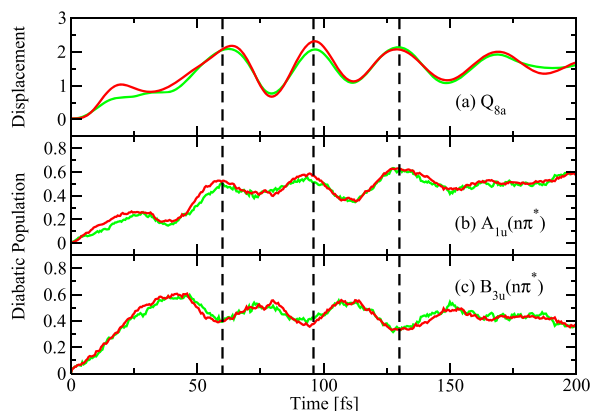

FIG. 8. Time-dependent displacement of the dimensionless Q_{8a} mode (a) in comparison with populations of the diabatic $A_{1u}(n\pi^*)$ (b) and $B_{3u}(n\pi^*)$ (c) states obtained with full-dimensional ADC(2) simulations. The red and green lines are calculated with the LZSH and LD-FSSH methods, respectively. The dashed lines mark the peaks of the population of the $A_{1u}(n\pi^*)$ state.

and $B_{3u}(n\pi^*)$ states rise within the first 40 fs, and then exhibit oscillations with a period of ~35 fs. The oscillatory features are similar to those obtained for the three-state model and reflect the electronic transitions in the diabatic representation driven by coherent dynamics in the Q_{8a} mode. This is confirmed by the time evolution of the dimensionless displacement of the Q_{8a} mode shown in Fig. 8. The maxima of the population probability of the $A_{1u}(n\pi^*)$ state and the minima of the population probability of the $B_{3u}(n\pi^*)$ state coincide with maxima of the displacement of the Q_{8a} mode.

V. CONCLUSIONS

In the present study, the nonadiabatic excited-state dynamics of pyrazine has been revisited within a model comprising three

excited electronic states and nine nuclear degrees of freedom. Exact numerical diabatic electronic population probabilities obtained for this model with the MCTDH method allow a quantitative assessment of the accuracy of two versions of TSH methods, FSSH and LZSH, by a direct comparison with the exact results. This comparison has become possible by the transformation of the adiabatic populations obtained with the SH methods to the diabatic representation. We first considered a reduced model comprising two excited electronic states, $B_{2u}(\pi\pi^*)$ and $B_{3u}(n\pi^*)$, and five normal modes. The results for this model show that both TSH methods are capable of providing a qualitatively correct description of the nonadiabatic population transfer dynamics dominated by the $B_{2u}(\pi\pi^*)/B_{3u}(n\pi^*)$ CI. In the three-state model, which includes the $A_{1u}(n\pi^*)$, $B_{2u}(\pi\pi^*)$, and $B_{3u}(n\pi^*)$ states and nine normal modes, the LZSH and FSSH diabatic populations are in very good agreement with the exact MCTDH results. An interesting feature of the three-state model are the population oscillations between the $A_{1u}(n\pi^*)$ and $B_{3u}(n\pi^*)$ states which reflect nonadiabatic electronic transitions driven by coherent dynamics in the Q_{8a} mode. We have shown that such vibrationally driven diabatic population oscillations are qualitatively reproduced by both TSH methods. Decoherence corrections to the FSSH method are not relevant for these models of the excited-state dynamics of pyrazine on the timescale of interest. Thanks to the availability of exact numerical time-dependent electronic population probabilities obtained with the MCTDH method for the three-state model, the accuracy of nonadiabatic TSH simulation methods could be tested in a far more realistic setting than previous tests of TSH methods against exact quantum dynamics results.

In addition to the reduced-dimensional model studies for pyrazine, full-dimensional on-the-fly simulations have been performed with the ADC(2) electronic-structure method to explore the performance of the TSH algorithms. The LZSH algorithm described in Sec. III A has been implemented for the first time for full-dimensional *ab initio* simulations. The accuracies of two FSSH variants, one in which the electronic wavefunction is propagated in the adiabatic basis (A-FSSH), and the other in which the propagation is performed in a locally diabatic basis (LD-FSSH), were compared. The time evolutions of the populations of the adiabatic states calculated using the LD-FSSH and LZSH methods are in excellent agreement. The decay time constant of the $B_{2u}(\pi\pi^*)$ state is also in excellent agreement with the experimental result. The LD-FSSH version of the FSSH method was found to be more accurate than the A-FSSH version for the case of ultrafast dynamics at conical intersections.

In good agreement with the three-state model study, the populations of the diabatic $A_{1u}(n\pi^*)$ and $B_{3u}(n\pi^*)$ states show clear oscillatory structures, whereas the adiabatic populations are essentially featureless. These findings imply that the three-state model of pyrazine with nine nuclear degrees of freedom provides an authentic description of the internal conversion dynamics of pyrazine on ultrafast time scales.

In the present implementation of the full-dimensional simulations, the LZSH calculations are only slightly (10%) faster than the FSSH calculations. However, pyrazine is a relatively small molecule that may not be representative for the comparison of the computational efficiencies of the LZSH and FSSH methods. Therefore, applications of the LZSH and FSSH methods to nonadiabatic processes

in large systems (e.g., organic semiconductors or biomolecules) are necessary to access the relative computational efficiency of the LZSH and FSSH methods.

SUPPLEMENTARY MATERIAL

See supplementary material for descriptions of the different integration schemes for the TDSE and a figure comparing the adiabatic populations calculated with the different integration schemes. Two figures comparing the adiabatic populations calculated with the LZSH method and LD-FSSH method with and without decoherence corrections for the three-state model and full-dimensional pyrazine.

ACKNOWLEDGMENTS

REFERENCES

[1] *Conical Intersections: Electronic Structure, Dynamics and Spectroscopy*, edited by W. Domcke, D. R. Yarkony, and H. Köppel (World Scientific, Singapore, 2004).

[2] *Conical Intersections: Theory, Computation and Experiment*, edited by W. Domcke, D. R. Yarkony, and H. Köppel (World Scientific, Singapore, 2011).

[3] H. Nakamura, *Nonadiabatic Transition: Concepts, Basic Theories and Applications* (World Scientific, 2012).

[4] D. R. Yarkony, Chem. Rev. **112**, 481 (2012).

[5] W. Domcke and D. R. Yarkony, Annu. Rev. Phys. Chem. **63**, 325 (2012).

[6] *Multidimensional Quantum Dynamics*, edited by H.-D. Meyer, F. Gatti, and G. A. Worth (Wiley-VCH Verlag GmbH & Co. KGaA, Weinheim, Germany, 2009).

[7] M. Barbatti, Wiley Interdiscip. Rev.: Comput. Mol. Sci. **1**, 620 (2011).

[8] J. C. Tully, J. Chem. Phys. **137**, 22A301 (2012).

[9] B. F. E. Curchod and T. J. Martínez, Chem. Rev. **118**, 3305 (2018).

[10] M. H. Beck, A. Jäckle, G. Worth, and H.-D. Meyer, Phys. Rep. **324**, 1 (2000).

[11] O. Vendrell, F. Gatti, and H.-D. Meyer, J. Chem. Phys. **127**, 184303 (2007).

[12] I. Kondov, M. Čížek, C. Benesch, H. Wang, and M. Thoss, J. Phys. Chem. C **111**, 11970 (2007).

[13] I. R. Craig, M. Thoss, and H. Wang, J. Chem. Phys. **127**, 144503 (2007).

[14] C. R. Evenhuis and U. Manthe, J. Phys. Chem. A **115**, 5992 (2011).

[15] T. Hammer, M. D. Coutinho-Neto, A. Viel, and U. Manthe, J. Chem. Phys. **131**, 224109 (2009).

[16] T. Hammer and U. Manthe, J. Chem. Phys. **136**, 054105 (2012).

[17] M. Nest and H.-D. Meyer, J. Chem. Phys. **117**, 10499 (2002).

[18] A. N. Beyer, J. O. Richardson, P. J. Knowles, J. Rommel, and S. C. Althorpe, J. Phys. Chem. Lett. **7**, 4374 (2016).

[19] M. T. Cvitaš and S. C. Althorpe, J. Chem. Theory Comput. **12**, 787 (2016).

[20] G. W. Richings, C. Robertson, and S. Habershon, J. Chem. Theory Comput. **15**, 857 (2018).

[21] G. W. Richings and S. Habershon, J. Chem. Phys. **148**, 134116 (2018).

[22] T. J. Martinez and R. D. Levine, J. Chem. Phys. **105**, 6334 (1996).

[23] M. Ben-Nun and T. J. Martínez, Adv. Chem. Phys. **121**, 439 (2002).

[24] B. Mignolet and B. F. E. Curchod, J. Chem. Phys. **148**, 134110 (2018).

[25] G. A. Worth, M. A. Robb, and I. Burghardt, Faraday Discuss. **127**, 307 (2004).

[26] G. W. Richings, I. Polyak, K. Spinlove, G. A. Worth, I. Burghardt, and B. Lasorne, Int. Rev. Phys. Chem. **34**, 269 (2015).

[27] H. R. Hudock, B. G. Levine, A. L. Thompson, H. Satzger, D. Townsend, N. Gador, S. Ullrich, A. Stolow, and T. J. Martínez, J. Phys. Chem. A **111**, 8500 (2007).

[28] D. Mendive-Tapia, B. Lasorne, G. A. Worth, M. A. Robb, and M. J. Bearpark, J. Chem. Phys. **137**, 22A548 (2012).

[29] B. Lasorne, M. A. Robb, and G. A. Worth, Phys. Chem. Chem. Phys. **9**, 3210 (2007).

[30] G. W. Richings and G. A. Worth, Chem. Phys. Lett. **683**, 606 (2017).

[31] B. F. E. Curchod, A. Sisto, and T. J. Martínez, J. Phys. Chem. A **121**, 265 (2017).

[32] J. C. Tully and R. K. Preston, J. Chem. Phys. **55**, 562 (1971).

[33] J. E. Subotnik, A. Jain, B. Landry, A. Petit, W. Ouyang, and N. Bellonzi, Annu. Rev. Phys. Chem. **67**, 387 (2016).

[34] L. Wang, A. Akimov, and O. V. Prezhdo, J. Phys. Chem. Lett. **7**, 2100 (2016).

[35] J. C. Tully, J. Chem. Phys. **93**, 1061 (1990).

[36] E. R. Bittner and P. J. Rossky, J. Chem. Phys. **103**, 8130 (1995).

[37] B. J. Schwartz, E. R. Bittner, O. V. Prezhdo, and P. J. Rossky, J. Chem. Phys. **104**, 5942 (1996).

[38] C. Zhu, S. Nangia, A. W. Jasper, and D. G. Truhlar, J. Chem. Phys. **121**, 7658 (2004).

[39] C. Zhu, A. W. Jasper, and D. G. Truhlar, J. Chem. Theory Comput. **1**, 527 (2005).

[40] G. Granucci and M. Persico, J. Chem. Phys. **126**, 134114 (2007).

[41] B. R. Landry and J. E. Subotnik, J. Chem. Phys. **135**, 191101 (2011).

[42] F. Plasser, G. Granucci, J. Pittner, M. Barbatti, M. Persico, and H. Lischka, J. Chem. Phys. **137**, 22A514 (2012).

[43] S. Fernandez-Alberti, A. E. Roitberg, T. Nelson, and S. Tretiak, J. Chem. Phys. **137**, 014512 (2012).

[44] L. Wang and O. V. Prezhdo, J. Phys. Chem. Lett. **5**, 713 (2014).

[45] C. Zener, Proc. R. Soc. London, Ser. A **137**, 696 (1932).

[46] L. D. Landau, Phys. Z. Sowijet. **1**, 51 (1932).

[47] L. D. Landau, Phys. Z. Sowijet. **2**, 46 (1932).

[48] E. E. Nikitin and S. Y. Umanskii, *Theory of Slow Atomic Collisions*, Springer Series in Chemical Physics (Springer Berlin Heidelberg, Berlin, Heidelberg, 1984), Vol. 30.

[49] J. N. Murrell and S. D. Bosanac, *Introduction to the Theory of Atomic and Molecular Collisions* (Wiley & Sons, Chichester, 1989).

[50] A. K. Belyaev and O. V. Lebedev, Phys. Rev. A **84**, 014701 (2011).

[51] W. Xie and W. Domcke, J. Chem. Phys. **147**, 184114 (2017).

[52] M. G. D. Nix, A. L. Devine, B. Cronin, R. N. Dixon, and M. N. R. Ashfold, J. Chem. Phys. **125**, 133318 (2006).

[53] G. M. Roberts, A. S. Chatterley, J. D. Young, and V. G. Stavros, J. Phys. Chem. Lett. **3**, 348 (2012).

[54] A. Ferretti, G. Granucci, A. Lami, M. Persico, and G. Villani, J. Chem. Phys. **104**, 5517 (1996).

[55] A. K. Belyaev, W. Domcke, C. Lasser, and G. Trigila, J. Chem. Phys. **142**, 104307 (2015).

[56] W. Xie, W. Domcke, S. C. Farantos, and S. Y. Grebenshchikov, J. Chem. Phys. **144**, 104105 (2016).

[57] I. Yamazaki, T. Murao, T. Yamanaka, and K. Yoshihara, Faraday Discuss. Chem. Soc. **75**, 395 (1983).

[58] J. Kommandeur, W. A. Majewski, W. L. Meerts, and D. W. Pratt, Annu. Rev. Phys. Chem. **38**, 433 (1987).

[59] Y. Okuzawa, M. Fujii, and M. Ito, Chem. Phys. Lett. **171**, 341 (1990).

[60] R. Schneider and W. Domcke, Chem. Phys. Lett. **159**, 61 (1989).

[61] U. Manthe and H. Köppel, J. Chem. Phys. **93**, 1658 (1990).

[62] L. Seidner, G. Stock, A. L. Sobolewski, and W. Domcke, J. Chem. Phys. **96**, 5298 (1992).

[63] C. Woywod, W. Domcke, A. L. Sobolewski, and H. Werner, J. Chem. Phys. **100**, 1400 (1994).

[64] A. Raab, G. A. Worth, H.-D. Meyer, and L. S. Cederbaum, J. Chem. Phys. **110**, 936 (1999).

[65] V. Stert, P. Farmanara, and W. Radloff, J. Chem. Phys. **112**, 4460 (2000).

[66] Y.-I. Suzuki, T. Fuji, T. Horio, and T. Suzuki, J. Chem. Phys. **132**, 174302 (2010).

[67] U. Werner, R. Mitrić, T. Suzuki, and V. Bonačić-Koutecký, Chem. Phys. **349**, 319 (2008).

[68] G. Tomasello, A. Humeniuk, and R. Mitrić, J. Phys. Chem. A **118**, 8437 (2014).

[69] M. Sala, B. Lasorne, F. Gatti, and S. Guérin, Phys. Chem. Chem. Phys. **16**, 15957 (2014).

[70] U. Müller and G. Stock, J. Chem. Phys. **107**, 6230 (1997).

[71] M. Santer, U. Manthe, and G. Stock, J. Chem. Phys. **114**, 2001 (2001).

[72] R. Gherib, I. G. Ryabinkin, and A. F. Izmaylov, J. Chem. Theory Comput. **11**, 1375 (2015).

[73] A. Mandal, S. S. Yamijala, and P. Huo, J. Chem. Theory Comput. **14**, 1828 (2018).

[74] D. J. Tannor, *Introduction to Quantum Mechanics: A Time-Dependent Perspective* (University Science Books, 2007).

[75] J. Schirmer, Phys. Rev. A **26**, 2395 (1982).

[76] A. B. Trofimov and J. Schirmer, J. Phys. B: At., Mol. Opt. Phys. **28**, 2299 (1995).

[77] M. Wormit, D. R. Rehn, P. H. Harbach, J. Wenzel, C. M. Krauter, E. Epifanovsky, and A. Dreuw, Mol. Phys. **112**, 774 (2014).

[78] A. Dreuw and M. Wormit, Wiley Interdiscip. Rev.: Comput. Mol. Sci. **5**, 82 (2015).

[79] TURBOMOLE V7.0 2015, a development of University of Karlsruhe and Forschungszentrum Karlsruhe GmbH, 1989–2007, TURBOMOLE GmbH, since 2007, available from http://www.turbomole.com.

[80] G. A. Meek and B. G. Levine, J. Phys. Chem. Lett. **5**, 2351 (2014).

[81] G. Granucci, M. Persico, and A. Toniolo, J. Chem. Phys. **114**, 10608 (2001).

[82] G. Worth, H.-D. Meyer, H. Köppel, L. Cederbaum, and I. Burghardt, Int. Rev. Phys. Chem. **27**, 569 (2008).

[83] J. C. Light, I. P. Hamilton, and J. V. Lill, J. Chem. Phys. **82**, 1400 (1985).

[84] M. Beck and H.-D. Meyer, Z. Phys. D: At., Mol. Clusters **42**, 113 (1997).

[85] A. A. Granovsky, J. Chem. Phys. **134**, 214113 (2011).

[86] M. Stener, P. Decleva, D. M. P. Holland, and D. A. Shaw, J. Phys. B: At., Mol. Opt. Phys. **44**, 075203 (2011).

[87] M. R. Silva-Junior, M. Schreiber, S. P. A. Sauer, and W. Thiel, J. Chem. Phys. **133**, 174318 (2010).

[88] M. Schreiber, M. R. Silva-Junior, S. P. A. Sauer, and W. Thiel, J. Chem. Phys. **128**, 134110 (2008).

[89] A. Bolovinos, P. Tsekeris, J. Philis, E. Pantos, and G. Andritsopoulos, J. Mol. Spectrosc. **103**, 240 (1984).

[90] I. C. Walker and M. H. Palmer, Chem. Phys. **153**, 169 (1991).

[91] W. H. Miller, J. Chem. Phys. **136**, 210901 (2012).

[92] T. Horio, R. Spesyvtsev, K. Nagashima, R. A. Ingle, Y.-i. Suzuki, and T. Suzuki, J. Chem. Phys. **145**, 044306 (2016).